



Supported by



## Accepted Article

**Title:** Understanding the Deactivation of Ag-ZrO<sub>2</sub>/SiO<sub>2</sub> Catalysts for the Single-Step Conversion of Ethanol to Butenes

**Authors:** Fan Lin, Vanessa Lebarbier Dagle, Austin D. Winkelman, Mark Engelhard, Libor Kovarik, Yilin Wang, Yong Wang, Robert Dagle, and Huamin Wang

This manuscript has been accepted after peer review and appears as an Accepted Article online prior to editing, proofing, and formal publication of the final Version of Record (VoR). This work is currently citable by using the Digital Object Identifier (DOI) given below. The VoR will be published online in Early View as soon as possible and may be different to this Accepted Article as a result of editing. Readers should obtain the VoR from the journal website shown below when it is published to ensure accuracy of information. The authors are responsible for the content of this Accepted Article.

**To be cited as:** *ChemCatChem* 10.1002/cctc.202001488

**Link to VoR:** <https://doi.org/10.1002/cctc.202001488>

# Understanding the Deactivation of Ag-ZrO<sub>2</sub>/SiO<sub>2</sub> Catalysts for the Single-Step Conversion of Ethanol to Butenes

Fan Lin,<sup>[a]</sup> Vanessa Lebarbier Dagle,<sup>\* [a]</sup> Austin D. Winkelman,<sup>[a], [b]</sup> Mark Engelhard,<sup>[a]</sup> Libor Kovarik,<sup>[a]</sup> Yilin Wang,<sup>[a]</sup> Yong Wang,<sup>[a], [b]</sup> Robert Dagle,<sup>\* [a]</sup> and Huamin Wang<sup>\* [a]</sup>

[a] Dr. F. Lin, Dr. V. L. Dagle, A. D. Winkelman, M. Engelhard, Dr. Libor Kovarik, Dr. Y. Wang, Prof. Dr. Y. Wang, Dr. R. Dagle, and Dr. H. Wang  
Institute for Integrated Catalysis,  
Pacific Northwest National Laboratory  
902 Battelle Blvd, Richland, Washington, 99354, USA  
E-mail: [vanessa.dagle@pnnl.gov](mailto:vanessa.dagle@pnnl.gov) (V. L. Dagle), [robert.dagle@pnnl.gov](mailto:robert.dagle@pnnl.gov) (R. Dagle), [huamin.wang@pnnl.gov](mailto:huamin.wang@pnnl.gov) (H. Wang)

[b] A. D. Winkelman, Prof. Dr. Y. Wang  
The Gene and Linda Voiland School of Chemical Engineering and Bioengineering  
Washington State University  
1505 Stadium Way, Pullman, Washington, 99164, USA

Supporting information for this article is given via a link at the end of the document.

**Abstract:** Ag-ZrO<sub>2</sub>/SBA-16 has recently been found to be efficient for catalyzing the single-step conversion of ethanol to butene (1- and 2-butene mixtures) in the presence of H<sub>2</sub>. The reaction proceeds via a cascading sequence of reactions over mixed metal and Lewis sites, with the catalyst composition tuned to selectively favor butene formation. However, the catalyst slowly deactivates when evaluated over long reaction times. In this work, we evaluated the lifetime of the Ag-ZrO<sub>2</sub>/SBA-16 catalyst system for ethanol-to-butene conversion at 325°C for up to 800 hours on stream. Several characterization techniques were used to elucidate the mechanism(s) by which catalyst deactivation occurs. Coke deposition, Ag particle sintering, and Ag<sup>0</sup>-to-Ag<sup>+</sup> oxidation state change were identified to be the major causes of catalyst deactivation. Coke deposits cover primarily Lewis acid sites which are responsible for aldol condensation, Meerwein-Ponndorf-Verley (MPV) reduction, and dehydration reactions. Ag particle sintering and Ag oxidation state change leads to a reduction in the number of metallic Ag sites responsible for the dehydrogenation/hydrogenation steps. The fresh catalyst likely experiences hydrothermal sintering in the early stage of reaction and permanently loses some active Lewis acid sites before reaching a new structural steady state. The deactivation of Lewis acid sites leads to a decrease in overall ethanol conversion, whereas the deactivation of the metallic Ag sites decreases the butene selectivity. For catalyst regeneration, oxidative calcination (at 500°C) followed by reduction (at 325°C) successfully removes all the coke species on the catalyst surface and restores the metallic Ag particles of the 4Ag-4ZrO<sub>2</sub>/SBA-16 catalysts.

## Introduction

Butenes are important industrial raw materials in the fuel industry for the production of jet fuels and blending components as octane enhancers<sup>[1]</sup> as well as in the polymer industry as the precursor for the commonly used copolymer polybutene.<sup>[2]</sup> Typically, butenes are obtained from fossil resources through catalytic cracking of heavier hydrocarbons produced during crude oil refining.<sup>[2b]</sup> To meet increasing demand, developing alternative routes for producing butenes are desirable, and biomass is

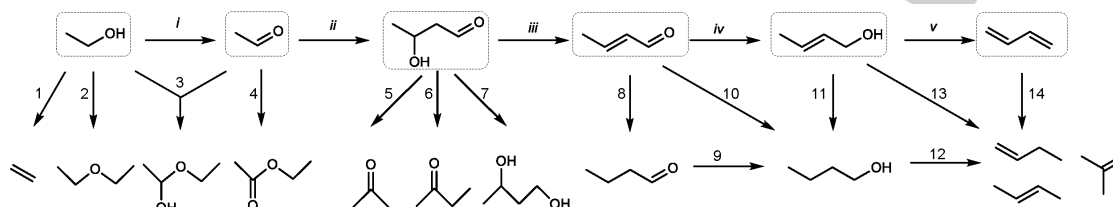
considered to be a promising alternative feedstock for their production.

In our recent economic assessment,<sup>[3]</sup> we show how profitability would be difficult to achieve when producing butene from ethanol, consisting potential revenues and feedstock cost based on market pricing (average 2015-2018 prices). However, reduction of the supply of naphtha-derived olefins such as butenes is expected because of a shift in lighter feedstock to steam crackers. Further, butene-rich mixed olefins can also be utilized as fuel precursors for producing distillate fuel. Renewable sourcing of distillate fuel (e.g., jet blendstock) offers regulatory incentives. Thus, various market drivers are in place for producing butene from renewable sources such as ethanol.

Butenes can be produced from ethanol via a process similar to the ethanol-to-butadiene (ETB) reaction, which was initially reported in the early 20<sup>th</sup> century, and has regained attention as a sustainable process as ethanol can be commercially produced from renewable biomass sources.<sup>[2a, 4]</sup> Scheme 1 (Steps *i-v*) depicts the generally accepted pathways for ETB conversion.<sup>[4f, 4g, 5]</sup> Ethanol is first dehydrogenated (Step *i*) to form acetaldehyde, which then undergoes aldol condensation and dehydration (Steps *i-iii*) to produce crotonaldehyde. Crotyl alcohol then is formed from the selective hydrogenation of the carbonyl bond in crotonaldehyde (Step *iv*). Finally, 1,3-butadiene is produced upon dehydration of crotyl alcohol (Step *v*). For ETB conversion, catalytic systems generally have acidic, basic, and/or redox active sites.<sup>[4d, 4f, 4g]</sup> Redox sites catalyze ethanol-to-acetaldehyde dehydrogenation and crotonaldehyde hydrogenation to crotyl alcohol, while acid and base sites are responsible for acetaldehyde condensation,<sup>[6]</sup> alcohol dehydration,<sup>[7]</sup> and MPV reduction for the crotonaldehyde to crotyl alcohol hydrogenation.<sup>[8]</sup> Varieties of binary and ternary metal oxide systems such as ZnO-Al<sub>2</sub>O<sub>3</sub><sup>[4h]</sup> and MgO-SiO<sub>2</sub> have been studied for ETB reactions.<sup>[9]</sup> To promote the dehydrogenation of ethanol and increase the yield of butadiene, promoters with redox properties (e.g., Ag, Cu, Ni, and Au)<sup>[4a, 4d, 10]</sup> are introduced. Among the metal-promoted oxide catalyst system for ETB conversion, Ag/ZrO<sub>2</sub>/SiO<sub>2</sub> has been found to have exceptional performance, with high butadiene selectivity (70%) while maintaining high conversion (>99%).<sup>[4a, 4d]</sup> Butenes are

## FULL PAPER

considered byproducts from dehydration of over-hydrogenated alcohol intermediates (Steps 8–13) and/or hydrogenation of butadiene (Step 14) in the ETB process. Therefore, promotion of ethanol-to-butene conversion in a process similar to the ETB process can be achieved by introducing or leveraging the hydrogenation functionality (e.g., Ag and Cu) in catalysts by adding H<sub>2</sub> as a reactant. This has been demonstrated by our recent work on Ag-ZrO<sub>2</sub>/SiO<sub>2</sub> catalysts.<sup>[11]</sup> The reaction mechanism for ethanol to butenes was elucidated through

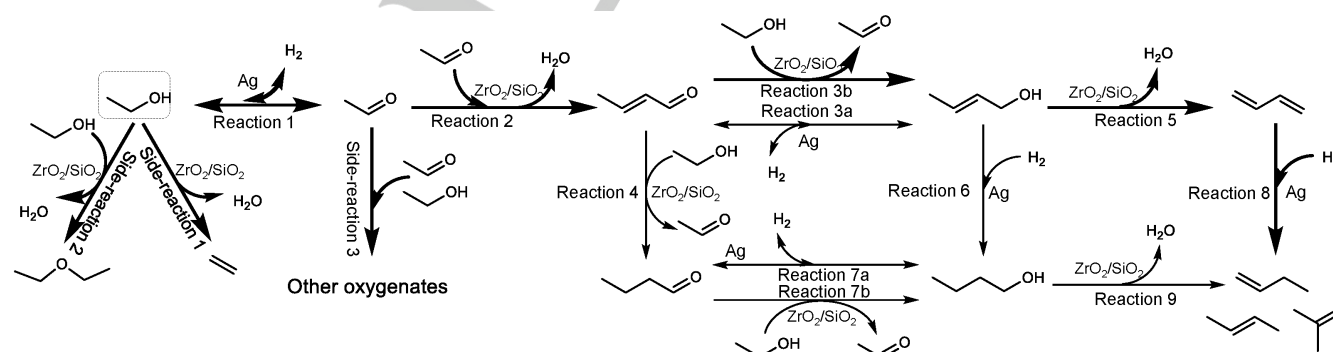


**Scheme 1.** Reaction network and the main byproducts of ETB conversions (reactions *i*–*v*) and the products (in boxes) represent the generally accepted reaction pathway toward butadiene. (Modified from the literature<sup>[49]</sup>.)

Catalyst stability is crucial to successful commercializing of the ethanol-to-butene (or butadiene) process. Because of the complexity of the reaction and many possible byproducts in ethanol-to-butadiene/butene conversion, maintaining the desired product selectivity over sustained time-on-stream is critical. This requires managing the deactivation of active sites while preserving the required balance between different types of sites that affect product selectivity. It is believed that coke deposition is the primary deactivation mode for ETB catalysts.<sup>[4f, 12]</sup> It is also known that catalyst stability can be improved through the addition of metal promoters on the catalysts and by introducing H<sub>2</sub> in the feed. However, there is usually a tradeoff between catalyst stability and butadiene selectivity when metal promoters are added to ETB catalyst systems. Sushkevich et al.<sup>[4d]</sup> compared a series of ZrO<sub>2</sub>/SiO<sub>2</sub> oxide catalysts with Ag, Cu, and Ni used as metal promoters. The Ni promoted catalyst showed the highest stability because it effectively cracks coke precursors, whereas the Ag and Cu promoted catalysts were less stable but had much higher yields of butadiene when compared to the Ni promoted catalyst. Our previous work<sup>[4a, 11]</sup> investigated the deactivation of Ag-ZrO<sub>2</sub>/SiO<sub>2</sub> catalysts in butadiene production. When the

reaction was performed in N<sub>2</sub>, ethanol conversion decreased from 100% to 80% within 20 hours on stream because of site blocking by coke deposition, but the butadiene selectivity remained stable at 70%. Introducing H<sub>2</sub> in the feed improved the catalyst stability by suppressing coke formation, but the butadiene selectivity decreased because of hydrogenation of butadiene to butene. Although similar metal-promoted oxide catalysts can be used for both butadiene and butene production, the specific reaction conditions and site requirements vary, and therefore, the deactivation mechanisms could be different under these circumstances.

In this work, we report the performance and properties of Ag-ZrO<sub>2</sub>/SBA-16 catalysts after 800 hours' time-on-stream for ethanol-to-butene conversion. We combined multiple characterization methods to elucidate the mechanisms of Ag-ZrO<sub>2</sub>/SBA-16 catalyst deactivation. Rationale for how the deactivation mechanisms affect the ethanol to butene reaction network was ascertained. Finally, we identified a suitable catalyst regeneration protocol for the system.



**Scheme 2.** Reaction steps for ethanol-to-butene conversion over 4Ag-4ZrO<sub>2</sub>/SBA-16 catalysts (thick arrows represent the predominant reactions while thin arrows represent minor or possible reactions).

## FULL PAPER

## Results and Discussion

Stability of 4Ag-4ZrO<sub>2</sub>/SBA-16 for ethanol-to-butene conversion

The 4Ag-4ZrO<sub>2</sub>/SBA-16 catalyst was efficient for conversion of ethanol to butene-rich hydrocarbon products. Scheme 2 depicts the major pathways of the relevant desired and side reactions, which was proposed by referring to literatures about ethanol-to-butadiene conversion<sup>[4f, 4g, 5, 13]</sup> and our previous study on ethanol-to-butene conversion.<sup>[11]</sup> In the scheme, thick arrows represent the predominant reaction pathways while thin arrows refer to minor or possible pathways. These reaction pathways combine catalytic hydrogenation/dehydrogenation and acid-base catalysis on the metal-acid multifunctional catalysts. In the major route of ethanol-to-butene conversion, ethanol first undergoes dehydrogenation (Reaction 1, Scheme 2), which leads to the formation of acetaldehyde. Acetaldehyde C-C coupling via aldol

condensation and dehydration (Reaction 2, Scheme 2) forms crotonaldehyde, which is the C<sub>4</sub> intermediate. Crotonaldehyde then undergoes C=O bond hydrogenation (Reactions 3a or 3b, Scheme 2) followed by dehydration (Reaction 5, Scheme 2) to form butadiene. Linear butenes (typically an equal distribution between trans-2, cis-2, and 1-butene with little to no isobutene) are produced upon the further hydrogenation of butadiene (Reaction 8, Scheme 2). Alternatively, as a minor route, complete hydrogenation of the C=C (Reactions 4 and 6, Scheme 2) and C=O bonds (Reactions 7a or 7b, Scheme 2) of crotonaldehyde produces butanol that then produces butene after an additional dehydration step (Reaction 9, Scheme 2). In parallel, side reactions of ethanol, including the mono-molecular dehydration to ethylene (Side-reaction 1, Scheme 2) and bimolecular dehydration to diethyl ether (Side-reaction 2, Scheme 2), occur. In addition, acetaldehyde also is consumed by a series of complicated side reactions (including aldol condensation, esterification, hydrolysis, ketonization, etc.) that lead to the production of various oxygenated side products such as ethyl acetate, acetic acid, and acetone (Side-reaction 3, Scheme 2)

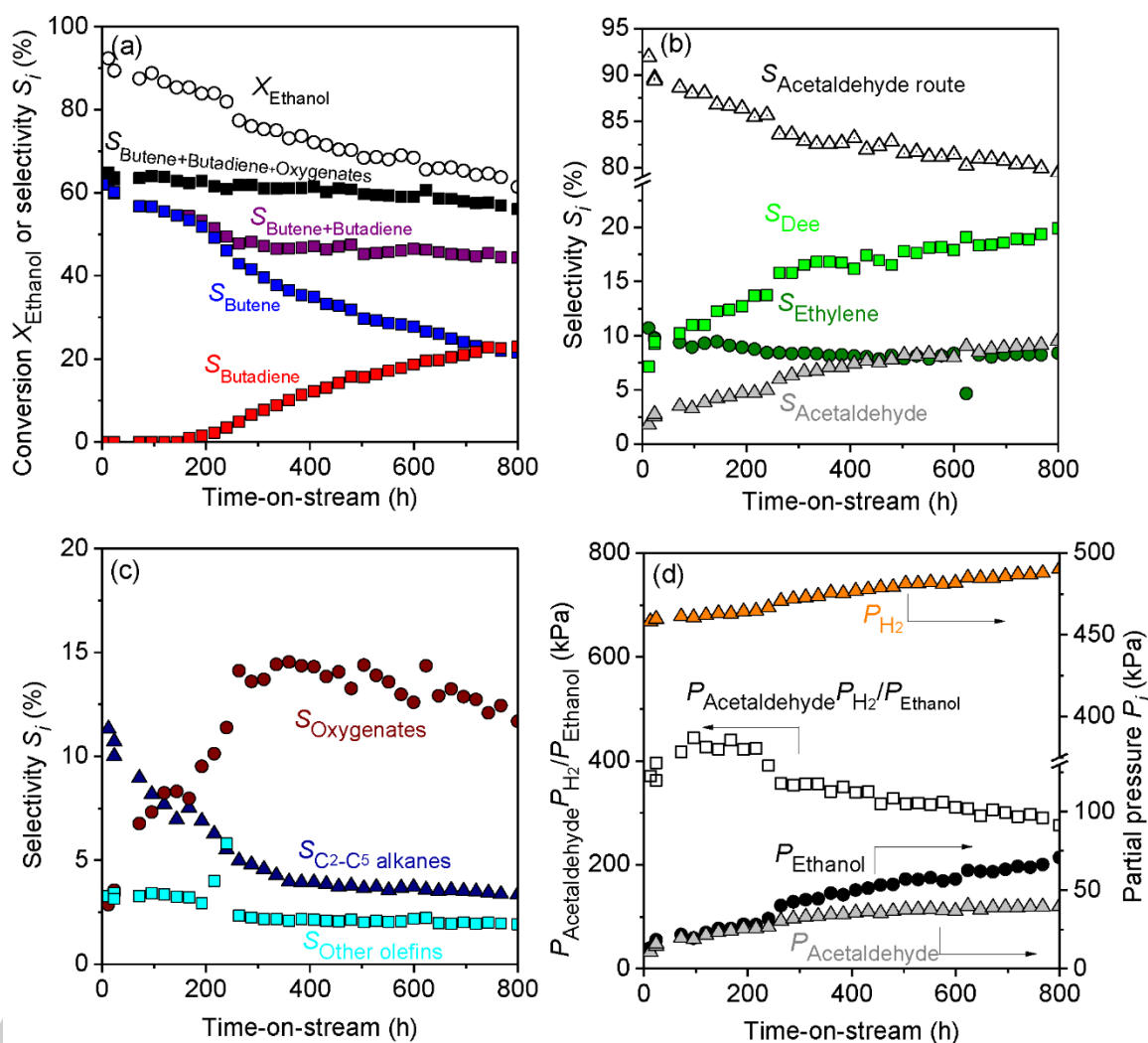


**Figure 1.** Ethanol conversion and selectivities for butene and butadiene (a); selectivities of primary products acetaldehyde, ethylene, and diethyl ether (b); selectivities of byproducts: oxygenates, C<sub>2</sub>-C<sub>5</sub> alkanes, and other olefins (c); and partial pressure ratio  $P_{\text{Acetaldehyde}} P_{\text{H}_2} / P_{\text{Ethanol}}$  (d) as a function of time-on-stream over 4Ag-4ZrO<sub>2</sub>/SBA-16 (325°C, 0.23 hr<sup>-1</sup>, 690 kPa; feed: 24 mol% P<sub>Ethanol</sub> in H<sub>2</sub>).

## FULL PAPER

The reactivity of 4Ag-4ZrO<sub>2</sub>/SBA-16 was measured for 800 hours on stream. Figure 1 shows the ethanol conversion ( $X_{\text{Ethanol}}$ ) and product selectivities ( $S_i$ ,  $i$ =product) as a function of time-on-stream. The stability of the catalysts was significantly improved in the presence of H<sub>2</sub> (ethanol conversion decreased from 90% to 60% after 800 hours of reaction), in comparison to the ETB process conducted in N<sub>2</sub> reported in our previous work [4a] (where ethanol conversion decreased from 100% to 80% within 20 hours on stream). However, the catalyst still suffers from slow deactivation, as the ethanol conversion and butene selectivity continue to decrease with time-on-stream (Figure 1a).

Figure 1b shows the yields of primary reaction products, intermediates, and side products. These include the ethanol dehydrogenation product acetaldehyde (Reaction 1, Scheme 2) and the two ethanol dehydration side products ethylene and diethyl ether (Side-reactions 1 and 2, Scheme 2, respectively). Acetaldehyde, as an intermediate, will convert further to butadiene, butene, oxygenates, and some other alkanes and alkenes. The total selectivity of acetaldehyde and the subsequent products ( $S_{\text{Acetaldehyde route}}$ ) are also shown in Figure 1b. The selectivity of unconverted acetaldehyde from ethanol dehydrogenation ( $Y_{\text{Acetaldehyde}}$ ) increased slowly before 500 hours on stream and then remains stable, as the decreasing ethanol conversion (Figure 1a) results in an increase of ethanol partial pressure ( $P_{\text{Ethanol}}$ ) (Figure 1d). It is worth noting that the partial pressure ratio  $P_{\text{Acetaldehyde}}P_{\text{H}_2}/P_{\text{Ethanol}}$  also remained relatively stable (Figure 1d), suggesting the ethanol-acetaldehyde interconversion was largely controlled by equilibrium (Reaction 1). The accurate value of the ethanol dehydrogenation equilibrium constant at 325°C is not available in literatures for comparison.

However, upon extrapolating the equilibrium constants measured by different researchers in the temperature range of 223-263 °C,[14] we estimated the equilibrium constant to be 2-8 atm at 325°C (see Figure S3 in SI). The  $P_{\text{Acetaldehyde}}P_{\text{H}_2}/P_{\text{Ethanol}}$  ratio of 270-440 kPa (2.7-4.3 atm) is within that equilibrium constant range, confirming the quasi-equilibrium hypothesis. In terms of the two dehydration side reactions, increasing ethanol pressure ( $P_{\text{Ethanol}}$ ) with time-on-stream promoted the bimolecular dehydration pathway forming diethyl ether (Side-reaction 2) [15], resulting in its increasing selectivity  $S_{\text{Dee}}$ . Conversely, the unimolecular dehydration pathway leading to ethylene formation (Side-reaction 1, Scheme 2) was independent of the ethanol pressure [15b]. This means that ethylene selectivity  $S_{\text{Ethylene}}$  decreased in parallel with ethanol conversion, which reflects catalyst deactivation.

The secondary reactions of acetaldehyde produced butadiene, butene, and oxygenated byproducts (Side-reaction 3, Scheme 2). Figure 1a shows the total selectivity of these products ( $S_{\text{Butene}} + S_{\text{Butadiene}} + S_{\text{Oxygenates}}$ ) decreased in parallel with the overall ethanol conversion  $X_{\text{Ethanol}}$ , suggesting that the loss of acetaldehyde conversion accounted for the loss of overall ethanol conversion. Initially, the selectivity of the desired product butene  $S_{\text{Butene}}$  was above 50%, but it decreased over time to 15% at 800 hours on stream. In contrast, butadiene formation was observed at 200 hours on stream before continuously increasing to more than 15% at 800 hours on stream. These inverse trends indicate a continuous loss of hydrogenation activity for butadiene-to-butene conversion.

**Table 1.** Physical and chemical properties of the fresh, spent, and regenerated 4Ag-4ZrO<sub>2</sub>/SBA-16 catalysts

Sample	Fresh (F0h)	Spent 5 hrs (S5h)	Spent 300 hrs (S300h)	Spent 800 hrs (S800h)	Regen 300 hrs (R300h)	Regen 800 hrs (R800h)
Surface area [a] (m <sup>2</sup> g <sup>-1</sup> )	518	491	486	422	485	498
Pore volume [a] (cm <sup>3</sup> g <sup>-1</sup> )	0.85	0.80	0.83	0.72	0.81	0.81
Ag size (chemisorption) [b] (nm)		4.4	4.8	6.8		
Ag size (TEM) [c] (nm)	2.8	3.3	3.3	4.0	4.0	4.0
Ag dispersion (TEM) [d] (%)	35.7	30.3	30.3	25.0	25.0	25.0
Lewis acid site density [e] (μmol g <sup>-1</sup> )	88	50	29	11	38	36
Metal site/acid site ratio [f]	0.41	0.61	1.04	2.27	0.66	0.69
Coke content (wt. %)	CHN [g]	-	1.8	3.0	-	-
	TGA [h]	-	1.4	2.9	3.8	-

[a] Measured by the Brunauer, Emmett, and Teller method (degassing at 150 °C for 12 hours). [b] Ag particle size (d) as calculated from chemisorption experiments where dispersion (D) was estimated assuming a Ag metal content of 4 wt.%, and assuming  $d = 100/D$  and spherical Ag particles. [c] Average Ag crystallite size (d) as estimated from the TEM microscopy. [d] Ag dispersion (D) as estimated using the average crystallite size (d) obtained from TEM microscopy, and assuming  $d=100/D$  and spherical Ag crystallites. [e] Measured by NH<sub>3</sub>-TPD (NH<sub>3</sub> adsorption temperature 100 °C). [f] Ratio of Ag dispersion (D), as estimated from TEM, and acid site ratio as determined by NH<sub>3</sub>-TPD. [g] Determined by carbon-hydrogen-nitrogen elemental analysis. [h] Determined from thermogravimetric analysis (TGA) based on the weight loss above 400 °C during TGA in flowing air.

Figure 1c shows the selectivity of the minor byproducts, including C<sub>2</sub>-C<sub>5</sub> alkanes, other olefins, and oxygenates (mostly ethyl acetate, acetic acid, acetone, butanol, and butyraldehyde). While the alkanes and olefins both continuously decreased with time-

on-stream, selectivity of oxygenates ( $S_{\text{Oxygenates}}$ ) increased within the first 300 hours on stream and then began a decreasing trend through the end of the reaction period. Because acid sites catalyzed the formation of oxygenates that then were converted

## FULL PAPER

to hydrocarbons by hydrogenation reactions, such a transition at 300 hours on stream in the  $S_{\text{Oxygenates}}$  trend is an indicator of the change in the balance between hydrogenation activity and acid-catalysis activity.

Change of the acidity on  $\text{ZrO}_2/\text{SiO}_2$  mixed oxides

On the multifunctional catalyst  $4\text{Ag-4ZrO}_2/\text{SBA-16}$ , the acid sites are responsible for aldol condensation, MPV reduction, and dehydration steps during ethanol-to-butene conversion, as depicted in Scheme 2. The  $\text{ZrO}_2/\text{SiO}_2$  mixed-oxide component provides this acidity in the form of Lewis acid sites. As reported in our previous work, this acidity is influenced by the interaction between  $\text{ZrO}_2$  and  $\text{SiO}_2$ , and SBA-16 acts as an ideal support to provide an optimal balance of sites for butadiene and thus butene production.<sup>[4a]</sup> The DRIFTS spectra of pyridine adsorption on all the fresh, spent, and regenerated  $4\text{Ag-4ZrO}_2/\text{SBA-16}$  catalysts (Figure S1 in the Supplemental Information) confirms the predominance of Lewis acid sites on the catalysts. The possible routes of Lewis acid site loss during the reaction include collapse of the SBA-16 pore structure, sintering of  $\text{ZrO}_2$ , and fouling from coke formation.

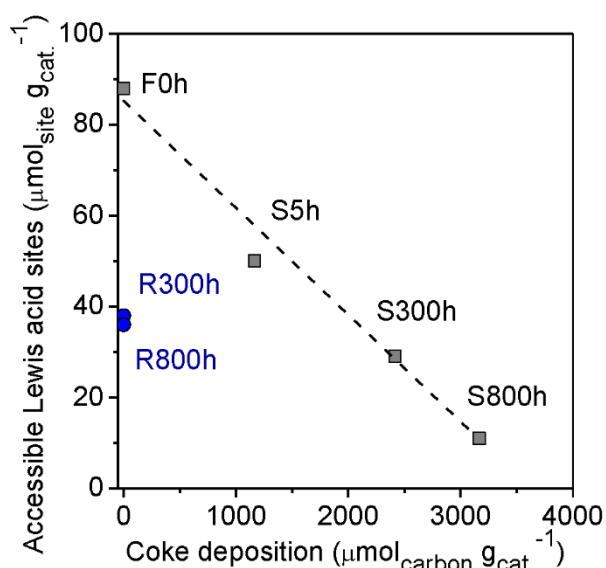


**Figure 2.** Amount of accessible Lewis acid sites on the fresh, spent, and regenerated  $4\text{Ag-4ZrO}_2/\text{SBA-16}$  catalysts as a function of coke deposition amount.

The loss of Lewis acid sites as a function of time-on-stream was confirmed by  $\text{NH}_3$ -TPD results listed in Table 1. We observed both reversible and irreversible loss of the active Lewis acid sites. As shown in Figure 2, the number of accessible Lewis acid sites on the fresh and spent catalysts decreased as coke deposition increased. In our recent work, we reported Raman Spectroscopy of spent catalysts after a shorter time on stream testing of ethanol to butenes indicating the presence of coke, with bands at  $1597$  and  $1360\text{ cm}^{-1}$  corresponding to the G band and the D band, respectively, of the graphitic carbon species.<sup>[11]</sup> However, the applied regeneration treatment ( $500\text{ °C}$ ,  $5\text{ mol}\%$   $\text{O}_2/\text{He}$  balance) only partially recovered the Lewis acid site acidity to  $36\text{--}38\text{ }\mu\text{mol g}^{-1}$  in comparison to the fresh catalyst ( $88\text{ }\mu\text{mol g}^{-1}$ ), even though regeneration removed a majority of deposited coke species from

the catalysts, as shown in Figure 2 and Table 1. While we attribute the reversible loss of Lewis acid sites to coke formation, the irreversible Lewis acid site loss is tentatively attributed to irreversible changes in catalyst texture/structure, such as the collapse of SBA-16 pore structure and/or sintering of  $\text{ZrO}_2$  on the surface of the catalyst.

The SBA-16 support was found to be relatively stable during the reaction. Figure 3 presents the XRD patterns of the fresh, spent, and regenerated catalysts. No indicative change in the  $\text{SiO}_2$  was observed, meaning that the SBA-16 support remains amorphous after 800 hours on stream. As listed in Table 1, the catalyst surface area decreased slightly from  $518\text{ m}^2\text{ g}^{-1}$  for fresh catalyst to  $486$  and  $422\text{ m}^2\text{ g}^{-1}$  for the spent samples after 300 hours and 800 hours on stream, respectively. Similarly, we observed a slight decrease in pore volume in the spent catalysts (from  $0.85$  to  $0.72\text{ cm}^3\text{ g}^{-1}$ ). These surface area or pore volume losses primarily were caused by coke deposition as they were mostly recovered upon re-calcination ( $500\text{ °C}$ ,  $5\%\text{ O}_2/\text{He}$ ). We speculate the irreversible loss of Lewis acid sites could be attributed to sintering or crystallization of the  $\text{ZrO}_2$ , as  $\text{ZrO}_2$  is present as amorphous  $\text{Zr}^{4+}$  patches in the fresh samples.<sup>[4a]</sup>

As shown in Figure 3, none of the fresh, spent, and regenerated  $4\text{Ag-4ZrO}_2/\text{SBA-16}$  catalysts show characteristic peaks for  $\text{ZrO}_2$ , suggesting that  $\text{ZrO}_2$  likely exists as widely dispersed amorphous patches on the SBA-16 support. Such  $\text{ZrO}_2$  patches were confirmed already by TEM and XRD analysis on the fresh  $\text{Ag-ZrO}_2/\text{SiO}_2\text{-636}$  catalysts in our previous work.<sup>[4a]</sup> Although none of the spent and regenerated  $4\text{Ag-4ZrO}_2/\text{SBA-16}$  catalysts showed any crystallized  $\text{ZrO}_2$  (Figure 3), we speculate that the irreversible loss of Lewis acid sites was caused by the shrinking of the  $\text{ZrO}_2$  patches upon sintering.

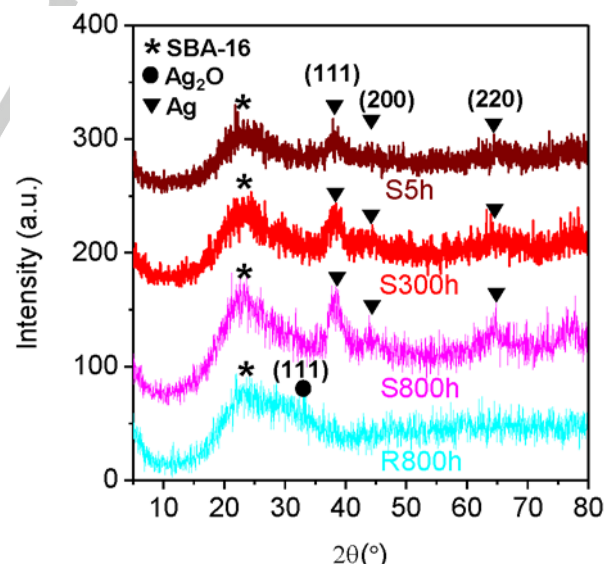


**Figure 3.** XRD spectra of the spent catalyst after 5 (S5h), 300 (S300h), and 800 hours (S800h) on stream, and of the catalyst regenerated and reduced after 800 hours on stream (R800h).

The catalyst was prepared by calcination at  $500\text{ °C}$  for 4 hours; therefore, it is unlikely that the regeneration treatment at  $500\text{ °C}$  would cause further sintering of  $\text{ZrO}_2$ .  $\text{ZrO}_2$  sintering could have

## FULL PAPER

occurred under hydrothermal conditions (at 325 °C, up to 20 vol.% of steam) during the initial stages of the reaction (i.e., within the first 10 hours), because water was generated as a byproduct of ethanol conversion. Oxide materials become less stable under hydrothermal conditions due to hydrolysis from H<sub>2</sub>O at high temperatures.<sup>[16]</sup> After the hydrothermal sintering of ZrO<sub>2</sub> in the early stages of reaction, the ZrO<sub>2</sub>/SiO<sub>2</sub> structure likely reaches a new steady state containing 36–38 μmol g<sup>-1</sup> of Lewis acid site. It is possible that such hydrothermal aging mechanisms also account for the minor loss of surface area and pore volume of the regenerated catalysts R300h and R800, in comparison to the fresh catalyst F0h (Table 1).

In summary, coke formation and hydrothermal sintering of the ZrO<sub>2</sub> patches are the likely routes for Lewis acid site loss on 4Ag-4ZrO<sub>2</sub>/SBA-16. Hydrothermal sintering of the ZrO<sub>2</sub> occurs in the early stages of the reaction, resulting in the irreversible loss of 57% of the Lewis acid sites on the surface. Additionally, the accumulation of coke species on the catalyst causes continuous Lewis acid site loss that is reversible upon re-calcination.

## Change of Ag sites

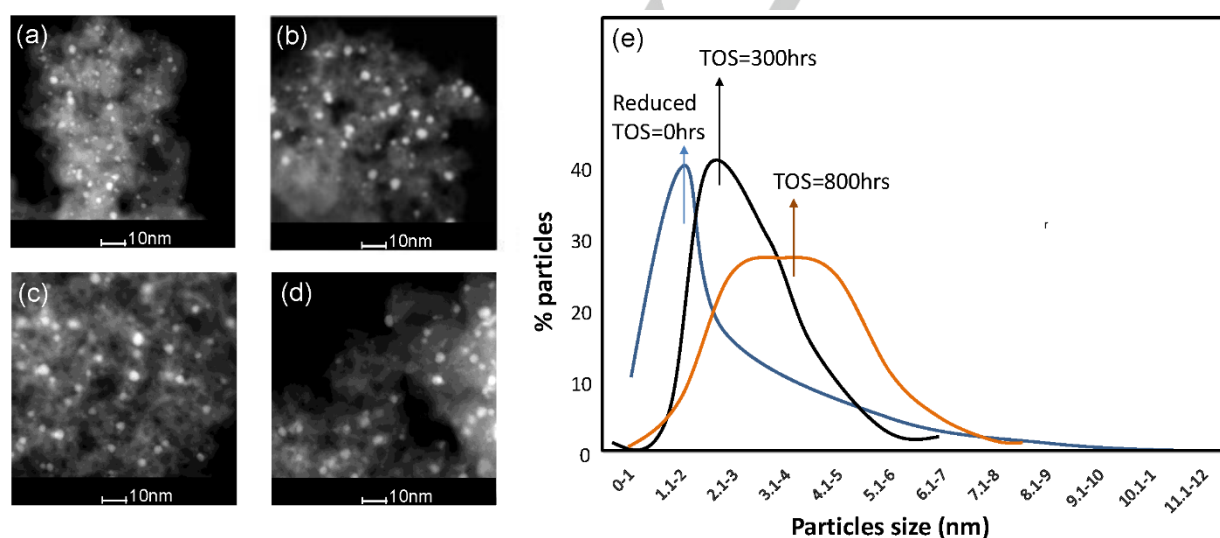


**Figure 4.** TEM analysis of the (a) fresh 4Ag-4ZrO<sub>2</sub>/SBA-16 catalyst, the spent samples after (b) 5 hours, (c) 300 hours, and (d) 800 hours on stream, and (e) Ag particle size distribution profiles

Another reason for Ag site deactivation is the change of oxidation state, from metallic silver to silver oxide.<sup>[18]</sup> We also performed *in situ* XPS analysis to understand how the Ag oxidation state changes with time-on-stream. Figure 5 shows the XPS spectra of Ag3d region for the fresh and spent samples. The freshly reduced sample (F0h) shows the typical binding energy for metallic Ag<sup>0</sup> at 368.0 eV (Ag3d<sub>5/2</sub>).<sup>[19]</sup> For the spent samples, the peak shifts to lower binding energies as the reaction time increases. This indicates that metallic Ag is progressively oxidized during the reaction and that the ratio of metallic-to-oxidized Ag particles decreases with time-on-stream.<sup>[19]</sup> We note that while oxidation of the Ag particles occurs, much of the metallic Ag<sup>0</sup> also likely remains. The Ag oxidation that does occur primarily happens during the first several hours of reaction. The spent samples after 300 and 800 hours on stream have similar binding energies of

In ethanol-to-butene conversion, the metallic Ag particles<sup>[17]</sup> are responsible for first enabling the dehydrogenation of ethanol to acetaldehyde (Reaction 1, Scheme 2) and then hydrogenation of the later intermediate butadiene to butene (Reaction 8, Scheme 2). As discussed in previous sections, the hydrogenation activity of the 4Ag-4ZrO<sub>2</sub>/SBA-16 catalysts decrease during the reaction due to the change of Ag sites. Two routes of Ag active site deactivation were identified. First, the growth of Ag particle size led to a decrease of accessible Ag sites. As shown in Figure 3, the diffraction peaks of the metallic Ag particle sharpen as time-on-stream increases, suggesting that the Ag particles grow with time. This trend of Ag particle size growth is consistent with our O<sub>2</sub>-H<sub>2</sub> titration measurements as listed in Table 1. Additionally, detailed TEM analysis, shown in Figure 4, also illustrates how the Ag particle size slightly increases with time-on-stream. As shown in Table 1, the average Ag particle size increases from 2.8 nm (fresh) to 4.0 nm (800 hours on stream). In addition to the increase of average Ag particle size, Ag particle size distribution also broadens with time-on-stream, as shown in Figure 4e. The two regenerated catalysts both have a Ag particle size of 4.0 nm, which is similar to the particle size in spent sample after 800 hours on stream, as shown in Table 1. This is likely an indication that the particle size growth slows down for larger Ag particles.

367.5 and 367.4 eV, respectively. Taken together, Ag particles do get oxidized under reaction conditions, primarily occurring during the first several hours on stream, which we attribute to the distribution of Ag metal oxidation states achieving an equilibrium.

In summary, over long reaction times, the hydrogenation activity of Ag sites on the fresh 4Ag-4ZrO<sub>2</sub>/SBA-16 catalyst is deactivated via two routes: partial oxidation and particle sintering of Ag. Partial Ag oxidation reached a steady state after 300 hours on stream, whereas sintering gradually slowed down as the particle size increased. Regeneration treatment by calcination and reduction could restore the Ag<sup>0</sup> oxidation state, but the increased Ag particle size was not re-dispersed by re-calcination at 500 °C.

## FULL PAPER

**Mechanism of 4Ag-4ZrO<sub>2</sub>/SBA-16 deactivation in ethanol-to-butene conversion**

Through catalytic performance analysis and detailed catalyst characterizations, we identified three routes of catalyst deactivation for 4Ag-4ZrO<sub>2</sub>/SBA-16 catalysts in ethanol-to-butene conversion.

1. Loss of Lewis acid sites by coke formation and hydrothermal sintering of ZrO<sub>2</sub> patches
2. Loss of surface Ag sites due to Ag particle growth
3. Transformation of Ag oxidation state from metallic Ag<sup>0</sup> into ionic Ag<sup>+</sup>.

Lewis acid sites mainly catalyze the series of reactions that convert acetaldehyde to butadiene, whereas the metallic Ag sites are responsible for the hydrogenation/dehydrogenation reactions, including ethanol dehydrogenation and butadiene hydrogenation. Lewis acid sites also play a minor role in catalyzing the hydrogenation/dehydrogenation reactions.

The continuous loss of Lewis acid sites directly leads to the continuous decrease of overall ethanol conversion. This is because the first step ethanol to acetaldehyde is in equilibrium and the Lewis acid sites catalyze the primary reactions of the ethanol-acetaldehyde reactant lump, including acetaldehyde-to-butadiene conversion (Reactions 2, 3b, and 5) and the two routes of ethanol dehydration (Side reactions 1 and 2), as well as the acetaldehyde side reactions (Side-reaction 3), as depicted in Scheme 2. As a result, the overall ethanol conversion and total selectivity of the acetaldehyde-derived C<sub>4</sub> hydrocarbons ( $S_{\text{Butene}} + S_{\text{Butadiene}}$ ) decreased upon deactivation of Lewis acid sites (Figure 1a).

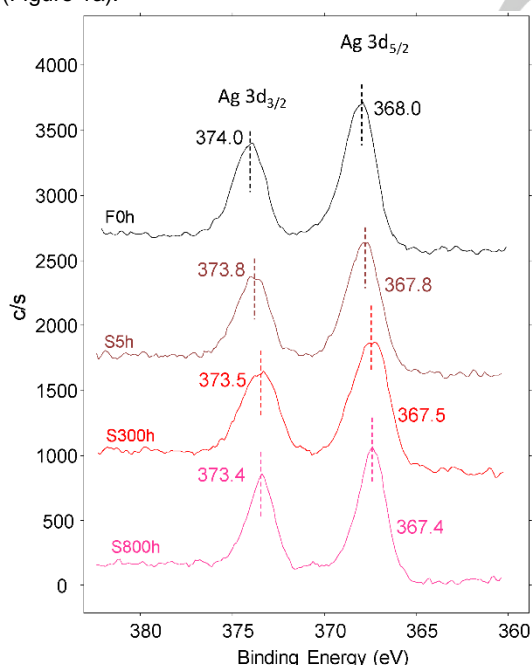


**Figure 5.** High-resolution XPS spectra of Ag3d region for the fresh (F0h) and spent samples after 5 hours (S5h), 300 hours (S300h), and 800 hours (S800h) on stream

On the other hand, the deactivation of Ag sites mainly influences product selectivities. First, Ag site deactivation has little impact on ethanol-to-acetaldehyde conversion. As shown in Scheme 2, the first step of ethanol dehydrogenation to acetaldehyde proceeds via reversible dehydrogenation catalyzed by Ag sites (Reaction 1). The relatively stable  $P_{\text{Aldehyde}}P_{\text{H}_2}/P_{\text{Ethanol}}$  ratio (Figure 1d) over long reaction times indicates that quasi-equilibrium likely is established among ethanol, acetaldehyde, and H<sub>2</sub> [14]. This ethanol-acetaldehyde equilibrium is largely maintained in the presence of excessive H<sub>2</sub> co-feed, regardless of the partial loss of Ag sites, likely because of the fast rate of ethanol-acetaldehyde interconversion on Ag sites.

Ag site deactivation, however, does harm C=C bond hydrogenation reactivity (Reactions 4, 6, and 8, Scheme 2) as required for butene formation, leading to the decrease of butene selectivity and increase of butadiene selectivity as the reaction progresses. The lower activity of C=C bond hydrogenation on Ag catalysts in comparison to C=O bond hydrogenation was previously confirmed by theoretical calculation studies, which showed the former has higher activation barrier (57–79 kJ mol<sup>-1</sup> for C=C vs. 33–39 kJ mol<sup>-1</sup> for C=O).<sup>[20]</sup> Therefore, C=C hydrogenation is more sensitive to Ag site deactivation than ethanol-acetaldehyde interconversion. In addition to the decrease of the butene yield with time-on-stream, the C<sub>2</sub>-C<sub>5</sub> alkane yield also decreased due to the loss of C=C bond hydrogenation activity of the catalyst as Ag sites deactivated (Figure 1c). ZrO<sub>2</sub> also contributed to the butadiene hydrogenation forming butene with a slower rate than Ag, which was demonstrated by the ethanol-to-butene conversion on Ag-free ZrO<sub>2</sub>/SBA-16 catalyst in our previous work.<sup>[11]</sup> However, because the formation of butadiene is mainly contributed by ZrO<sub>2</sub> (Reactions 2, 3b and 5, Scheme 2), we believe the loss of ZrO<sub>2</sub> solely would not break the butadiene formation-hydrogenation balance and change the butene selectivity. Thus the deactivation of another hydrogenation site, Ag, must be the major cause for the butene selectivity decrease.

We found Lewis acid site deactivation from coke formation to be reversible. Oxidative treatment at 500 °C completely removes all of the coke from the catalysts. However, permanent loss of partial Lewis acid sites occurred, likely due to hydrothermal sintering of the highly dispersed ZrO<sub>2</sub> during the reaction. The calcination-reduction treatment also successfully recovers the hydrogenation activity of the Ag sites. However, the re-calcination step of the regeneration process (500 °C) leads to Ag particle growth (e.g. from 3.3 nm to 4.0 nm for the sample R300h, Table 1), probably because the long time exposure to the hydrothermal condition of reaction stream weakens the metal-support bonding and destabilizes the Ag particles, causing the growth of Ag particle under 500 °C re-calcination. Despite the permanent loss of some Lewis acid sites after regeneration, the catalyst performance for ethanol-to-butene conversion was mostly recovered after regeneration, expect for an increase in ethylene dehydration side-product, as reported in our previous work.<sup>[11]</sup> The reason for the increase of ethylene byproduct was not well understood. We speculate that this increase is possibly related to the restructuring of the Lewis acid sites upon hydrothermal sintering of ZrO<sub>2</sub> on the surface of the catalyst.

## FULL PAPER

## Conclusion

The 4Ag-4ZrO<sub>2</sub>/SBA-16 catalyst system efficiently converts ethanol into butene in the presence of H<sub>2</sub> co-feed. However, catalysts deactivation occurs over the course of extended time-on-stream. We have identified three routes of catalyst deactivation.

1. Loss of Lewis acid sites by coke formation and hydrothermal sintering of ZrO<sub>2</sub> patches
2. Loss of surface Ag sites due to Ag particle growth
3. Transformation of Ag oxidation state from metallic Ag<sup>0</sup> into ionic Ag<sup>+</sup>.

Lewis acid sites are responsible for aldol condensation, MPV reduction, and dehydration reactions, so the loss of Lewis acid sites leads to the decrease of the overall ethanol conversion but does not affect the product selectivities. The deactivation of metallic Ag sites significantly impacts C=C bond hydrogenation activity for butene formation, resulting in a decrease in butene selectivity. The fast and equilibrated ethanol-acetaldehyde interconversion in the presence of excessive H<sub>2</sub>, however, is not influenced by the partial deactivation of the Ag sites.

Regeneration treatment via oxidation (at 500 °C) followed by hydrogenation (at 350 °C), successfully removes all coke species on the catalyst surface and restores the oxidation state of Ag to Ag<sup>0</sup> of the 4Ag-4ZrO<sub>2</sub>/SBA-16 catalysts. The fresh catalyst likely experiences hydrothermal sintering in the early stages of the reaction and permanently loses some Lewis acid sites before reaching a new structural steady state.

## Experimental Section

## Catalyst preparation

The 4Ag-4ZrO<sub>2</sub>/SBA-16 catalyst was synthesized by incipient wetness impregnation of SBA-16 (ACS Materials) with silver nitrate powder and zirconyl nitrate solution dissolved in deionized water. After impregnation, the catalyst was dried at 110 °C for 8 hours and calcined for 4 hours at 500 °C. The fresh 4Ag-4ZrO<sub>2</sub>/SBA-16 sample was reduced in 10% H<sub>2</sub>, at 325 °C for 1 hour before characterization and labeled as F0h. The spent samples obtained after 5, 300, and 800 hours on stream were labeled as S5h, S300h, and S800h respectively. A portion of the spent S300h and S800h samples was regenerated by treatment under 5% O<sub>2</sub>/N<sub>2</sub> at 500 °C for 5 hours and were labeled as R300h and R800h, respectively. Note that the regenerated samples for characterization were not reduced prior to characterization unless indicated in the text.

## Catalyst activity evaluations

Reactivity tests for the conversion of ethanol to butene-rich olefins were conducted in a 6.35-mm outer diameter (inner diameter = 4.57 mm) fixed-bed reactor loaded with 2.0 g of catalyst. A K-type thermocouple was placed in middle of the reactor to measure the catalyst bed temperature. To minimize temperature gradients, an electrical resistance heating block was installed on the reactor. Prior to testing, the catalyst was first activated in situ at 450 °C for 8 hours under 120 ml min<sup>-1</sup> of N<sub>2</sub>. Then, the temperature was cooled to 325 °C, and the catalyst was reduced under 100 ml min<sup>-1</sup> of 10% H<sub>2</sub>/N<sub>2</sub> for 1 hour. Prior to operation, the system was purged under H<sub>2</sub> for about 10 minutes, and the pressure was increased to 690 kPa. Ethanol fed into the system using an ISCO syringe pump was converted to the gas phase using a vaporizer consisting of 6.6-mm inner diameter steel tubing filled with quartz beads. Catalyst conversion and selectivity were

measured at 325 °C, 690 kPa, and a WHSV<sub>Ethanol</sub> of 0.23 g<sub>Ethanol</sub> g<sub>Catalyst</sub><sup>-1</sup> hr<sup>-1</sup>. Hydrogen typically was used as the carrier gas (24 mol% P<sub>Ethanol</sub> in H<sub>2</sub>). A knockout pot placed directly downstream of the reaction zone was used to collect liquid product. Gaseous effluent was analyzed online using an Inficon micro-GC (Model 3000A) equipped with MS-5A, Plot U, alumina, OV-1 columns, and a thermal conductivity detector. Liquid samples collected from the knockout pot were analyzed separately ex situ using liquid chromatography. For catalyst regeneration studies, the catalyst was oxidized under 5% O<sub>2</sub>/He for 5 hours at 500 °C prior to a re-reduction of the catalyst. To prevent exposure to the outside environment after each reaction was completed, spent catalysts were cooled to room temperature under 100 ml min<sup>-1</sup> of inert N<sub>2</sub> in the reactor system before being isolated by airtight ball valves on either side of the reactor and immediately transferred to a glove box under inert Ar before being collected for characterization. Ethanol conversion, products selectivities, and product yields were calculated as shown in equations (1), (2), and (3) below. The carbon balance was typically within 10%.

$$\text{Ethanol conversion (\%)} = \frac{100 \times (\text{moles ethanol})_{\text{in}} - (\text{moles ethanol})_{\text{out}}}{(\text{moles ethanol})_{\text{in}}} \quad (1)$$

$$\text{Carbon selectivity product } i \text{ (\%)} = \frac{100 \times \text{moles of carbon in product } i}{\text{total carbon moles in identified products}} \quad (2)$$

$$\text{Carbon yield product } i \text{ (\%)} = 100 \times \text{Ethanol conversion} \times \text{Carbon selectivity product } i \text{ (3)}$$

## Catalyst characterization

X-ray diffraction (XRD) spectra were measured with a Physical Electronics Quantera Scanning X-Ray Microprobe using a focused monochromatic Al K $\alpha$  X-ray (1486.7 eV) source for excitation and a spherical section analyzer. The surface areas and pore volumes were measured with a Quantachrome autosorb iQ gas sorption system. Before measurements were made, the samples were degassed at 150 °C in vacuum for 12 hours.

The type of acid site (i.e., Lewis or Brønsted) was determined by pyridine adsorption at 150 °C followed by Fourier-transform infrared analysis using a DRIFT cell. Before the measurement, the samples were pretreated in situ by ramping the DRIFT cell cup temperature to 150 °C in flowing He and holding the temperature at 150 °C for 30 minutes. Acid site densities were measured by NH<sub>3</sub>-temperature programmed desorption (TPD) in quartz plug flow reactors (inner diameter = 10 mm). The samples (~60–80 mg) were pretreated by purging with 300 ml min<sup>-1</sup> N<sub>2</sub> for 1 hour at 100 °C. NH<sub>3</sub> adsorption was performed at 100 °C by flowing 300 ppm NH<sub>3</sub>/N<sub>2</sub> (300 ml min<sup>-1</sup>) until saturation was achieved, followed by purging in 300 ml min<sup>-1</sup> N<sub>2</sub> for 2 hours. The TPD measurements were performed by ramping to 600 °C at 10 °C min<sup>-1</sup> in 300 ml min<sup>-1</sup> N<sub>2</sub>. The desorbed species in the effluent were quantified with an MKS MultiGas analyzer.

The H<sub>2</sub>-O<sub>2</sub> titration was conducted on Micromeritics AutoChem II chemisorption analyzer with a method similar to that in the literature.<sup>[21]</sup> The samples were first reduced in 10% H<sub>2</sub>/Ar (40 ml min<sup>-1</sup>, 10 °C min<sup>-1</sup>) at 400 °C for 2 hours. Then He gas was passed over the sample for 1 hour. After cooling to 170 °C in He, the O<sub>2</sub> (10% O<sub>2</sub>/He balance) adsorption experiment was performed, followed by flushing with He (40 ml min<sup>-1</sup>) before H<sub>2</sub> pulses (1 cm<sup>3</sup> of 10% H<sub>2</sub>/Ar balance) were introduced to titrate the Ag sites. Stoichiometric ratios for Ag:O<sub>2</sub> of 2 and Ag:H<sub>2</sub> of 0.667 were assumed.

Temperature gravimetry analysis was performed on a NETZSCH STA-409-CD simultaneous thermal analyzer. The samples were pretreated at 120 °C in 60 ml min<sup>-1</sup> air (zero grade) for 30 minutes, before ramping to 800 °C at 5 °C/minute.

Transmission electron microscopy (TEM) measurements were conducted with an FEI Titan 80–300 operated at 300 kV. All images were digitally recorded using a charge-coupled device camera and were analyzed using Gatan Microscopy Suite<sup>®</sup> software version 3.4.1. TEM images were

## FULL PAPER

collected from at least five different locations on the grid. In general, TEM sample preparation involved mounting powder samples on copper grids covered with lacey carbon support films and then immediately loading them into the TEM airlock to minimize an exposure to atmospheric O<sub>2</sub>. Before measurement, samples were reduced at 325 °C for 1 hour under 10% H<sub>2</sub>/N<sub>2</sub>. Ag dispersion was calculated from the Ag<sup>0</sup> particle size using the formula  $D\% = 100/d$  where D represents the dispersion and d stands for the Ag<sup>0</sup> particle size. At least 100 particles were analyzed to determine the Ag<sup>0</sup> particle size of each catalyst.

X-ray photoelectron spectroscopy (XPS) measurements were performed with a Physical Electronics Quantera Scanning X-ray Microprobe. For XPS analysis of spent catalysts, the catalytic reactor containing a spent catalyst was isolated to prevent exposure to air and immediately transferred to the XPS glove box where it was then removed from the reactor under inert Ar for analysis. Under vacuum, the powder catalysts were pressed into a 4 mm × 1 mm diameter holes machined into a custom 13 mm diameter stainless steel sample stub designed for use with a custom modified 8ULVAC PHI XPS sample platen. The custom sample platen and sample stub were pretreated with the loaded catalyst in He at 300 °C for 30 minutes and then placed into the XPS vacuum system. The Si 2p line at 103.5 eV was used for charge referencing.

## Acknowledgements

The authors gratefully acknowledge funding for this research, provided by the U.S. Department of Energy (DOE), Office of Energy Efficiency and Renewable Energy (EERE), Bioenergy Technologies Office (BETO). This work was done at the Pacific Northwest National Laboratory (PNNL), and in collaboration with the Chemical Catalysis for Bioenergy Consortium (ChemCatBio), a member of the Energy Materials Network (EMN). PNNL is a multi-program national laboratory operated for DOE by Battelle Memorial Institute. This work was also supported in part through the PNNL-WSU Distinguished Graduate Research Program for A.D.W, a student at Washington State University. Use of catalyst characterization equipment and computational resources was provided by a user proposal at the William R. Wiley Environmental Molecular Sciences Laboratory, which is a national scientific user facility sponsored by the DOE Office of Biological and Environmental Research and located at PNNL in Richland, WA. Finally, the authors thank Cary Counts for technical editing support.

The views and opinions of the authors expressed herein do not necessarily state or reflect those of the United States Government or any agency thereof. Neither the United States Government nor any agency thereof, nor any of their employees, makes any warranty, expressed or implied, or assumes any legal liability or responsibility for the accuracy, completeness, or usefulness of any information, apparatus, product, or process disclosed, or represents that its use would not infringe privately owned rights.

**Keywords:** ethanol • butene • butadiene • Ag-ZrO<sub>2</sub>/SiO<sub>2</sub> • deactivation

[1] M. A. Lilga, R. T. Hallen, K. O. Albrecht, A. R. Cooper, J. G. Frye, K. K. Ramasamy, US Patent 9,663,416.

- [2] a) V. Zacharopoulou, A. A. Lemonidou, *Catalysts* **2018**, *8*, 2; b) J. G. Speight, in *Environmental Organic Chemistry for Engineers* (Ed.: J. G. Speight), Butterworth-Heinemann, **2017**, pp. 87-151.
- [3] R. A. Dagle, A. D. Winkelman, K. K. Ramasamy, V. L. Dagle, R. S. Weber, *Ind. Eng. Chem. Res.* **2020**, *59*, 4843-4853.
- [4] a) V. L. Dagle, M. D. Flake, T. L. Lemmon, J. S. Lopez, L. Kovarik, R. A. Dagle, *Appl. Catal. B* **2018**, *236*, 576-587; b) M. D. Jones, *Chem. Cent. J.* **2014**, *8*, 53; c) C. Angelici, B. M. Weckhuysen, P. C. A. Bruijninx, *ChemSusChem* **2013**, *6*, 1595-1614; d) V. L. Sushkevich, I. Ivanova, V. V. Ordonskiy, E. Taarning, *ChemSusChem* **2014**, *7*, 2527-2536; e) G. O. Ezinkwo, V. P. Tretyakov, A. Aliyu, A. M. Ilolov, *ChemBioEng Rev.* **2014**, *1*, 194-203; f) G. Pomalaza, M. Capron, V. Ordonskiy, F. Dumeignil, *Catalysts* **2016**, *6*, 203; g) E. V. Makshina, M. Dusselier, W. Janssens, J. Degrève, P. A. Jacobs, B. F. Sels, *Chem. Soc. Rev.* **2014**, *43*, 7917-7953; h) S. K. Bhattacharyya, N. D. Ganguly, *J. Appl. Chem.* **1962**, *12*, 105-110.
- [5] T. Yan, W. Dai, G. Wu, S. Lang, M. Hunger, N. Guan, L. Li, *ACS Catal.* **2018**, *8*, 2760-2773.
- [6] a) J. Sun, R. A. L. Baylon, C. Liu, D. Mei, K. J. Martin, P. Venkatasubramanian, Y. Wang, *J. Am. Chem. Soc.* **2016**, *138*, 507-517; b) S. Wang, K. Goulas, E. Iglesia, *J. Catal.* **2016**, *340*, 302-320; c) J. D. Lewis, S. Van de Vyver, Y. Román-Leshkov, *Angew. Chem.* **2015**, *127*, 9973-9976; d) H. Zhang, M. Y. S. Ibrahim, D. W. Flaherty, *J. Catal.* **2018**, *361*, 290-302.
- [7] a) F. Lin, Y. Chen, L. Zhang, D. Mei, L. Kovarik, B. Sudduth, H. Wang, F. Gao, Y. Wang, *ACS Catal.* **2020**, *10*, 4268-4279; b) P. Kostestky, J. Yu, R. J. Gorte, G. Mpourmpakis, *Catal. Sci. Tech.* **2014**, *4*, 3861-3869; c) I. Carrizosa, G. Munuera, *J. Catal.* **1977**, *49*, 174-188; d) I. Carrizosa, G. Munuera, *J. Catal.* **1977**, *49*, 189-200.
- [8] a) T. Komanoya, K. Nakajima, M. Kitano, M. Hara, *J. Phys. Chem. C* **2015**, *119*, 26540-26546; b) H. Li, J. He, A. Riisager, S. Saravanamurugan, B. Song, S. Yang, *ACS Catal.* **2016**, *6*, 7722-7727; c) A. Corma, M. E. Domine, S. Valencia, *J. Catal.* **2003**, *215*, 294-304.
- [9] V. V. Ordonskiy, V. SushkevichIrina, L. I. Ivanova, US Patent US 8,921,635 B2.
- [10] a) S. Shylesh, A. A. Gokhale, C. D. Scown, D. Kim, C. R. Ho, A. T. Bell, *ChemSusChem* **2016**, *9*, 1462-1472; b) C. Angelici, M. E. Z. Velthoen, B. M. Weckhuysen, P. C. A. Bruijninx, *ChemSusChem* **2014**, *7*, 2505-2515.
- [11] V. L. Dagle, A. Winkelman, N. Jaegers, J. Hu, M. Engelhard, S. E. Habas, S. Akhade, V.-A. Glezakou, R. Rousseau, Y. Wang, R. A. Dagle, *ACS Catal.* **2020**, *10*, 10602-10613.
- [12] T. Yan, L. Yang, W. Dai, C. Wang, G. Wu, N. Guan, M. Hunger, L. Li, *J. Catal.* **2018**, *367*, 7-15.
- [13] V. L. Sushkevich, I. I. Ivanova, *Appl. Catal. B* **2017**, *215*, 36-49.
- [14] J. Happel, J. C. Chao, R. Mezaki, *J. Chem. Eng. Data* **1974**, *19*, 110-112.
- [15] a) M. A. Christiansen, G. Mpourmpakis, D. G. Vlachos, *ACS Catal.* **2013**, *3*, 1965-1975; b) J. F. DeWilde, H. Chiang, D. A. Hickman, C. R. Ho, A. Bhan, *ACS Catal.* **2013**, *3*, 798-807.

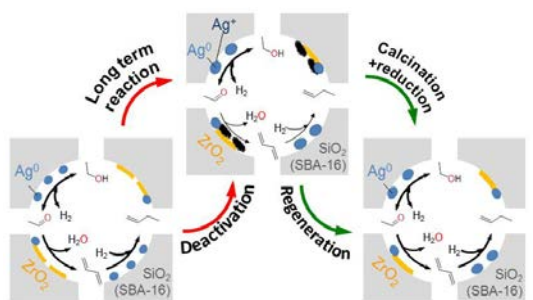
## FULL PAPER

- [16] H. Xiong, H. N. Pham, A. K. Datye, *Green Chem.* **2014**, *16*, 4627-4643.
- [17] a) V. L. Sushkevich, I. I. Ivanova, E. Taarning, *ChemCatChem* **2013**, *5*, 2367-2373; b) G. Vilé, D. Baudouin, I. N. Remediakis, C. Copéret, N. López, J. Pérez-Ramírez, *ChemCatChem* **2013**, *5*, 3750-3759.
- [18] M. Bron, D. Teschner, A. Knop-Gericke, F. C. Jentoft, J. Kröhnert, J. Hohmeyer, C. Volckmar, B. Steinhauer, R. Schlögl, P. Claus, *Phys.Chem.Chem.Phys.* **2007**, *9*, 3559-3569.
- [19] I. M. Arabatzis, T. Stergiopoulos, M. C. Bernard, D. Labou, S. G. Neophytides, P. Falaras, *Appl. Catal. B* **2003**, *42*, 187-201.
- [20] K. H. Lim, A. B. Mohammad, I. V. Yudanov, K. M. Neyman, M. Bron, P. Claus, N. Rösch, *J. Phys. Chem. C* **2009**, *113*, 13231-13240.
- [21] S. R. Seyedmonir, D. E. Strohmayer, G. L. Geoffroy, M. A. Vannice, H. W. Young, J. W. Linowski, *J. Catal.* **1984**, *87*, 424-436.

WILEY-VCH

Accepted Manuscript

## Entry for the Table of Contents



This work reveals the deactivation mechanisms of Ag-ZrO<sub>2</sub>/SBA-16 catalysts during the sustainable synthesis process of ethanol-to-butene conversion, guiding the deactivation mitigation and catalyst regeneration.

Institute and/or researcher Twitter usernames: ((optional))